Available online at www.sciencedirect.com
SCIENCE DIRECT®
International Journal of Heat and Mass Transfer 49 (2006) 4596–4607
International Journal of HEAT and MASS TRANSFER
www.elsevier.com/locate/ijhmt

Transient convective diffusion to a circular sink at finite Peclet number

Ondrej Wein [a,*], Valentin V. Tovcigrecko [a], Vaclav Sobolik [b]

[a] Institute of Chemical Process Fundamentals, ASCR, 16502 Praha 6, Czech Republic
[b] LMTAI, Pole Sciences, University of La Rochelle, 17042 La Rochelle Cedex, France

Received 7 March 2006
Available online 27 June 2006

Abstract

Theory by Geshev and Safarova [P.I. Geshev, N.S. Safarova, Angular and transient characteristics of circular electrochemical friction probes, Int. J. Heat Mass Transfer 42 (1999) 3183–3188] of transient mass transfer from shear flow to circular sink is checked over broad range of Peclet number by electrodiffusion experiments with varied sink radius (0.1–1 mm), shear rate (0.5–200 s^{-1}), and diffusivity (4×10^{-11}–7×10^{-10} $m^2\,s^{-1}$). This theory is confirmed within 2% accuracy for steady-state mass-transfer coefficients but transient characteristics are completely wrong. Area, perimeter, and transport length of circular probes are autocalibrated by fitting a semi-empirical model on the transient data at known shear rates. Well-calibrated probes provide data on diffusion coefficient and wall shear rate with accuracies of 2% and 5%, respectively.

Keywords: Edge effect at finite *Pe*; Electrodiffusion flow diagnostics; Transient convective diffusion

1. Introduction

1.1. Mass-transfer friction probes

Electrodiffusion (ED) experiment provides a unique method for mapping the local velocity gradient at a wall (wall shear rate) γ [1–3]. An ED friction probe is a two-electrode electrochemical cell in a streaming electrolyte solution, see Fig. 1. It consists of a large auxiliary electrode and a small working electrode (mass-transfer sink for the working depolarizer), embedded flush in an insulating wall. Electrochemical operating conditions (composition of the electrolyte solution, size and location of the both electrodes, electrochemical quality of their catalytic surfaces, and voltage U between them) should ensure the regime of limiting diffusion current (LDC regime), with the current i independent of small changes of U.

Basic mass-transfer theory [4] of ED probes assumes explicitly existence of a thin diffusion layer at the surface of working electrode and, tacitly, presence of a bulk with constant concentration c_B of the working depolarizer. Strictly speaking, the ED probes are sensitive to overall velocity field inside their diffusion layer. If the diffusion layer is thin enough, the only significant parameter of the near-wall velocity field is γ. The primary ED signal – steady-state total current i – can be expressed in the diffusion-layer (DL) approximation, $k \approx k_L$, according to well-known *Leveque* formula [1–4] for the heat/mass-transfer coefficient,

$$D(\gamma/9Dh)^{1/3}/\left(\frac{2}{3}\Gamma\left(\frac{4}{3}\right)\right) = k_L = i_L/Ac_B n\mathbf{F}. \quad (1)$$

Here, h stands for the equivalent transport length of ED probe in the flow direction [1]. With known bulk concentration, c_B, effective diffusion coefficient of the working depolarizer, D, and geometry of the probe, $\{A,h\}$, the formula (1) can be used for conversion of primary steady current data, i, onto wall shear rate, γ.

* Corresponding author. Tel.: +420 220 390 310; fax: +420 220 920 661.
E-mail addresses: wein@icpf.cas.cz (O. Wein), tovcigrecko@icpf.cas.cz (V.V. Tovcigrecko), vsobolik@univ-lr.fr (V. Sobolik).

0017-9310/$ - see front matter © 2006 Elsevier Ltd. All rights reserved.
doi:10.1016/j.ijheatmasstransfer.2006.05.002

Nomenclature

A area of probe, m^2
$b = 1.6272$ coefficient in Eq. (8a) for h of circular probe in shear flow
c concentration field of working depolarizer, mol m^{-3}
c_B bulk value of c, mol m^{-3}
$C = (D/\pi)^{1/2}$ Cottrell coefficient, Eq. (2), m $s^{-1/2}$
D effective diffusion coefficient of working depolarizer, m^2 s^{-1}
$n\mathbf{F}$ charge transferred by electrode consumption of working depolarizer, C mol^{-1}
h equivalent transport length of probe, m
$h'(y)$ lateral distribution of local transport lengths, m
$H = h/\lambda$ modified Peclet number, $H = 0.5424R(\gamma/D)^{1/2} = (Pe/13.597)^{1/2}$
$i = i(t)$ limiting diffusion current, A
i_{std} steady-state current, A
i_L steady-state limiting diffusion current in DL approximation, A
$k = i/Ac_B n\mathbf{F}$ mass-transfer coefficient, m s^{-1}
$k_L = \frac{3}{2}Lh^{-1/3}$ steady-state k in DL approximation (*Leveque*), m s^{-1}
k_{std} steady-state k, m s^{-1}
$k' = D\partial_z c|_{z=0}/c_B$, instantaneous local mass-transfer coefficient, m s^{-1}
$L = D\lambda^{-2/3}/\Gamma(4/3)$, Leveque coefficient, Eq. (5), $m^{4/3}$ s^{-1}
$N = k/k_L$ normalized mass-transfer coefficient
P perimeter of probe, m
$Pe \equiv 4R^2\gamma/D$ conventional Peclet number for a circular sink in shear flow
R nominal radius of circular probe, m
$Sh = 2Rk_{std}/D$ steady-state Sherwood number
Sh_0 Sh for natural convection, Eq. (25)
$Sh_L = 2Rk_L/D$ Sh for forced convection in DL approximation, Eq. (10)
t time from the start of voltage step, s
$T = tC^{-2}k_L^2$ normalized time
x, y, z longitudinal, transversal, and normal coordinates, m
x streamwise distance to the forward edge, m
β_0, β_∞ early-stage and steady-state corrections on edge effects
γ wall shear rate, s^{-1}
χ_C coefficient of the Cottrell asymptote, Eq. (2), A $s^{1/2}$
κ ratio of inner to outer radius in Couette viscometer, Eq. (20)
$\kappa_A, \kappa_P, \kappa_H$ corrections on non-ideal probe geometry, Eq. (18abc)
$\lambda = (9D/\gamma)^{1/2}$ convective-diffusion depth of edge border, m
ν kinematic viscosity, m^2 s^{-1}
Ω rotation speed of inner cylinder of the Couette viscometer, rad s^{-1}
DL diffusion layer
ED electro-diffusion
LDC limiting diffusion current

1.2. Potentiostatic transient and autocalibration

Potentiostatic transient process [5,6] is started by switching U from an equilibrium (zero current) value to a value ensuring the LDC regime. For an early stage of the transient process, $t \to 0$, the transient mass-transfer coefficient in the DL approximation, $k \approx Ct^{-1/2}$ can be expressed by the well-known *Cottrell* formula,

$$(D/\pi)^{1/2} = C = \chi_C/Ac_B n\mathbf{F}, \quad (2)$$

where $C \equiv \lim_{t\to 0} t^{1/2}k(t)$, $\chi_C \equiv \lim_{t\to 0} t^{1/2}i(t)$. This asymptotic formula, developed originally for a motionless solution, is valid also for an early stage of the transient process in moving liquid.

The concept of autocalibration [3,6] operates with D, which is determined from early stage of the transient process according to (2), and used subsequently in calculating wall shear rate γ according to (1). Even if the bulk concentration c_B and/or probe area A are not known with an extremely high accuracy, the value of γ calculated from

$$\gamma = \frac{8}{3}\Gamma^3\left(\frac{4}{3}\right)\pi^{-2}(c_B n\mathbf{F}A)hi_L^3\chi_C^{-4} = \frac{8}{3}\Gamma^3\left(\frac{4}{3}\right)\pi^{-2}hk_L^3C^{-4}, \quad (3)$$

may be still acceptable. Accuracy of the resulting γ depends, with an extreme sensitivity, both on the early-stage asymptote χ_C (*Cottrell*), and steady-state asymptote i_L (*Leveque*).

1.3. Problem statement

Primary signal in unsteady electrochemical voltamperic measurements – course of electrical current $i(t)$ – can be measured with extremely high accuracy but, on the other hand, its value depends on incredibly many factors. This circumstance makes any quantitative interpretation of primary data extremely difficult and forces many electrochemists to ignore fundamental theory and prefer various *ad hoc* calibration methods.

In the present study, we follow rather metrological approach. It consists in applying theory of convective diffusion in the way that reflects all rationally tractable factors, in particular the unsteady 3D edge effects at finite Peclet number and real geometry of working electrodes. The theory [7] for the ED probes of ideal circular shape is checked experimentally.

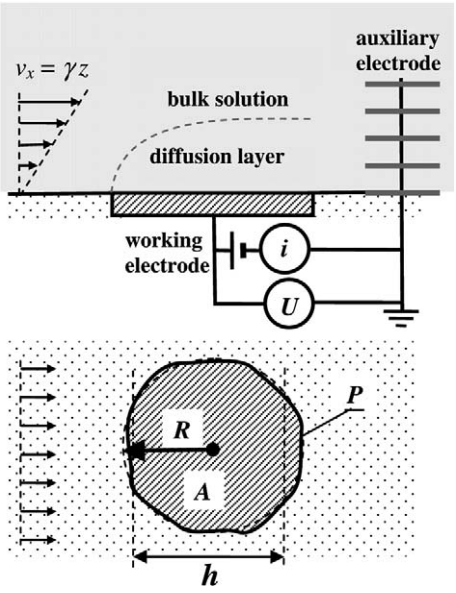

Fig. 1. Basic items of ED friction probe and geometry of circular working electrode: i – electric current; U- polarization voltage; γ – shear rate; R – nominal radius; A – area; P – perimeter; h – transport length, see Eq. (7).

A serious simplification in the present study consists in neglecting the *electrochemical transport resistances* like Ohm resistance and kinetics of electrode reaction at working electrode. This cannot be acceptable in an initial stage of the transient, when the mass-transfer theory predicts zero transport resistance. Consequently, the Cottrell asymptote (2) should be taken with some caution. The early-stage domain of the transient, where this simplified transient mass-transfer model is quantitatively acceptable, should be found experimentally.

2. Convective-diffusion theory of the transient process

Under LDC conditions, theory of the potentiostatic transient in an ED cell with the steady shear flow in x-direction along a solid planar wall $z = 0$ reduces to linear elliptic boundary-value problem of convective diffusion, $\partial_t c + \gamma z \partial_x c = D(\partial_{xx} + \partial_{yy} + \partial_{zz})c$ for the concentration field $c(x, y, z, t)$ of a working depolarizer. The initial/boundary conditions assume:

- constant bulk concentration everywhere before the start, $t < 0$;
- jump to zero concentration at the surface of the sink after the start, $t > 0$;
- zero diffusion flux to neighboring walls;
- constant bulk concentration anywhere in a far distance from the sink.

Due to zero concentration close to the active surface, the concentration gradient is normal to this surface, i.e. $\partial_x c = 0$, $\partial_y c = 0$. Neglecting $\partial_x c$, $\partial_y c$ everywhere, the elliptical boundary-value problem reduces to parabolic one, see (4a). This, so called diffusion-layer (DL) approximation, which corresponds to infinite Peclet number, is exposed first and corrected further for finite Peclet by including corrections on edge effect.

2.1. Diffusion-layer approximation: convective wave

The parabolic transport equation in aforementioned DL approximation,

$$\partial_t c + \gamma z \partial_x c = D \partial_{zz} c, \tag{4a}$$

is accompanied with boundary conditions at the semi-infinite rectangular domain (x, t, z):

$$c = c_B \quad (\text{for } x < 0 \text{ or } t < 0 \text{ or } z = \infty), \tag{4b}$$

$$c = 0 \quad (\text{for } x > 0 \text{ and } t > 0 \text{ and } z = 0), \tag{4c}$$

that include no characteristic size of a sink.

Because of the singular initial conditions in ($x = 0$, $z = 0$, $t = 0$), there are two different solutions to the transient problem. In addition to the *analytic* (continuously differentiable) results [8,9], there is a simple *weak* solution [10] with the following expression of local mass-transfer coefficients:

$$k'(x,t) = \begin{cases} k'_L(x) = Lx^{-1/3}; & x < (L/C)^3 t^{3/2} \\ k'_C(t) = Ct^{-1/2}; & x > (L/C)^3 t^{3/2} \end{cases} \tag{5}$$

that combines the transient uniformly accessible *Cottrell* asymptote $k'_C(t)$ and steady-state local *Leveque* asymptote $k'_L(x)$. These sub-domains are separated by the moving *convective wave* with the trajectory $x = (L/C)^3 t^{3/2}$, defined by $k'_L(x) = k'_C(t)$.

The resulting integral mass-transfer transient coefficient $k(t)$ for a strip of finite streamwise length h can be normalized by using the parameters C and $k_L = \frac{3}{2} L h^{-1/3}$:

$$N(T) = \begin{cases} T^{-1/2}(1 + \frac{1}{2}(T/T_0)^{3/2}); & T < T_0 \\ 1; & T > T_0 \end{cases}, \quad T_0^{-1/2} = \frac{2}{3}. \tag{6}$$

For ED probe of any convex shape [11], the transient $k(t)$ can be obtained simply by integrating local fluxes according to (5) over the surface A, $k(t) = A^{-1} \int\int_A k'(x,t) \mathrm{d}x \mathrm{d}y$, where x denotes longitudinal distance of a given point in the surface from the forward edge. With the shape given by lateral distribution of local transport lengths, $x \in (0; h'(y))$, $A = \int h'(y) \mathrm{d}y$, the steady-state (*Leveque*) asymptote, $k_L = A^{-1} \int\int_A L x^{-1/3} \mathrm{d}x \mathrm{d}y$, can still be expressed by formula (1), using the equivalent transport length h,

$$h = \left(\int h'(y) \mathrm{d}y \Big/ \int h'(y)^{2/3} \mathrm{d}y \right)^3. \tag{7}$$

For the circular ED probe of radius R, $h'(y) = 2(R^2 - y^2)^{1/2}$, it is [1,11]:

$$h = bR,$$

$$b = \left(\int_0^1 [2(1-s^2)]^{1/2} \mathrm{d}s \Big/ \int_0^1 [2(1-s^2)]^{1/3} \mathrm{d}s \right)^3 = 1.6272. \tag{8a,b}$$

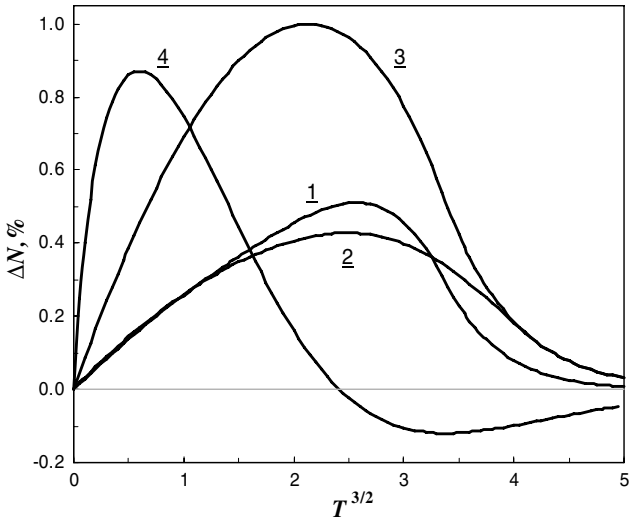

Fig. 2. Relative deviation $\Delta N = N_{anal}/N - 1$ of various approximations N from exact analytical solutions for the potentiostatic transient in DL approximation ($H = \infty$). 1. Weak solution (convective wave) for strip probes, $N = N_{weak}$, according to Eq. (6); 2. Weak solution (convective wave) for circular probes, $N = N_{weak}$, taken from [11]; 3. $N(T)$ according to (6) used for circular probes as an approximation; 4. $N(T) = (1 - \exp(-T^{5/3}))^{-3/10}$ from [2,6] used for circular probes as an approximation.

The analytic, N_{anal}, and weak, N_{weak}, solutions for the strip and circular ED probes are compared in Fig. 2, together with empirical approximations for the circular probes. It is not quite clear which of the solutions (analytical or weak) is a better asymptotic approximation to the unknown correct asymptote of the 3D problem (finite H) for $H \to \infty$.

Normalized transients $N(T)$ share by definition the common zero-order asymptotes, $N(T) \approx T^{-1/2}$ for $T \to 0$ and $N(T) \approx 1$ for $T \to \infty$, but their overall courses slightly differ for different shapes [11]. Anyway, (6) still gives a satisfactory approximation both to N_{anal} and N_{weak} for probes of any convex shape. As shown in Fig. 2, curve 3, the "convective wave" approximation according to (6) deviates from N_{anal} for the circular probe by less than 1%.

2.2. Steady-state 3D edge effect in shear flow

Contributions to the steady-state total LDC due to 2D forward and trailing edge effects on an infinite strip in shear flow were analytically first estimated by Newman, see e.g. [4]. An older numerical study [12] is not sufficiently sensitive to edge effects because of ignoring border singularities of the corner type [4]. The further analytical effort by numerous authors has been corrected and completed in [13].

The depths of border regions of a strip probe with important contribution of longitudinal diffusion can be estimated [4] by $\lambda = (9D/\gamma)^{1/2}$. The same estimate holds for the effect of lateral diffusion at the side border of rectangular probe [14]. These conclusions suggest a more suitable definition of Peclet number also for the circular probes:

$$H \equiv h/\lambda = (Pe/13.597)^{1/2}, \tag{9}$$

instead of the conventional $Pe = 4R^2\gamma/D$. The quantity H^{-1} directly gives the relative depth of the border with important edge effects. For $H > 1$, it is reasonable to operate with local (forward, trailing, lateral) edge effects while, for $H < 1$, the edge borders are overlapping and the notion of individual edge contributions losses any physical sense. The contribution of 3D diffusion at finite H for a class of geometrically similar ED probes in a shear flow can be expressed through a correction function

$$k_{std}/k_L = Sh/Sh_L = 1 + \beta_\infty(H), \tag{10}$$

where k_L stands for the DL estimate of actual k_{std} according to the full 3D theory. Sherwood number Sh for circular probes is based on the nominal diameter, see Nomenclature. Note the well-known [1,7] result $Sh_L = 2.0646H^{2/3} = 0.8650Pe^{1/3}$.

The numerical results about 3D steady-state convective diffusion for a circular ED probe in shear flow are given in [7] by an empirical formula that can be recalculated to the present notation as

$$\beta_\infty(H) = 1.0131H^{-1} - 0.2753H^{-4/3} + 0.0065H^{-2}. \tag{11}$$

Another asymptotic estimate of $\beta_\infty(H)$ at high H is given in [15],

$$\beta_\infty(H) = 0.893H^{-1}. \tag{12}$$

The asymptote for extremely low H, $b_\infty(H) \approx 1.2334H^{-2/3}$ follows from the known finite value of k for steady-state pure diffusion at $H = 0$, $k = (4/\pi)D/R$. Higher-order asymptotic expansion for $H \to 0$ is given in [13]:

$$\beta_\infty(H) = 1.2334H^{-2/3}(1 - 0.176H^3)/(1 - 0.374H). \tag{13}$$

Comparison of these estimates indicates that the correlation (11) of numerical data [7] could provide a reliable estimate of β_∞ for $H > 1$. An evident drawback of the empirical formula (11) lies in its contradiction with the analytical asymptotes (13) for extremely low H and disagreement with (12) for higher H. Unfortunately, the rough numerical Sh–Pe data, for their better or more consistent correlation than by (11), are not available. Note an inherent inaccuracy in [7] of about 0.1% due to incorrect DL approximation, written in [7] as $Sh_L = aPe^{1/3}$ with $a = 0.866$ instead of the correct $a = 0.8650$.

2.3. Transient edge effects in motionless liquid: Oldham asymptote

Using the analytic solution of the 2D transient problem in a motionless liquid for a semi-infinite sink separated by a straight line boundary from its insulating neighborhood [16], Oldham suggested an improved early-stage transient mass-transfer asymptote, $t \to 0$. The zero-order contribution, proportional to the sink area A, is the original Cottrellian term and the first-order contribution to edge effects is proportional to the sink perimeter P,

$$k(t) \approx Ct^{-1/2} + \frac{DP}{2A}. \tag{14}$$

This general asymptote is identical with the first two terms of the complete transient solution [17] for circular ED probe in a motionless liquid.

It is obvious from the solution (6) in DL approximation that the early stage of transient is identical with the (zero-order) Cottrellian asymptote for a motionless liquid, i.e. it does not depend on convection. The same holds for the (first-order) Oldham asymptote (14) at finite H. For an ED probe in steady shear flow with given k_L, the formula (14) can be normalized to:

$$N(T) \approx T^{-1/2} + \beta_0, \tag{15}$$

$$\beta_0 \equiv \frac{DP}{2Ak_L} = \frac{1}{3}\Gamma\left(\frac{4}{3}\right)\frac{Ph}{A}H^{-2/3}. \tag{16}$$

In particular, $\beta_0 = 0.9687\ H^{-2/3}$ for a geometrically ideal circular ED probe.

2.4. Overall transient process at finite Peclet number

Geshev and Safarova [7] claim to obtain a full numerical solution to the transient problem over a broad range of H. However, the empirical formulas used to represent the transient data in [7] are obviously wrong, as they:

- do not converge to a DL asymptote for $H \to \infty$;
- do not fit the Oldham asymptote at an early stage of transient;
- approach the steady-state asymptote from below instead from above.

Examples of incorrect predictions for various H are compared in Fig. 3 with correct results.

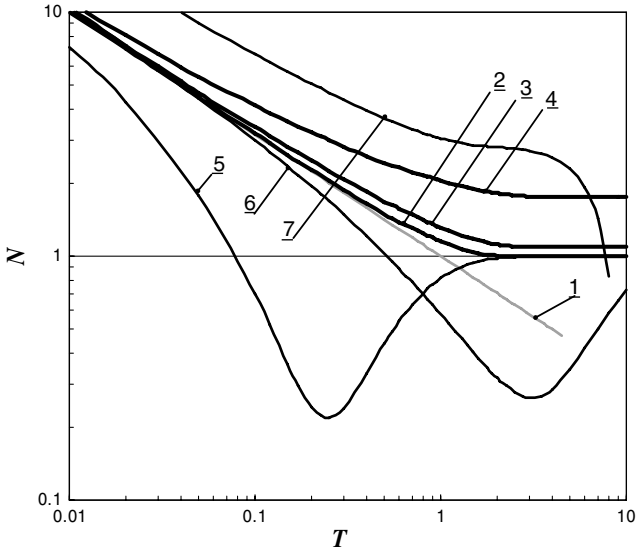

Fig. 3. Prediction [6] of the transient characteristics in comparison with the present experimental transient data. 1. Cottrell asymptote, $N = T^{-1/2}$; 2, 3, 4. Formula (17), confirmed by the present experiments, for $H = 1000$, 10, 1, resp.; 5, 6, 7. According to the formulas from [7]; for $H = 1000$, 10, 1, resp.

In conclusion, there is no reliable theoretical prediction of the complete potentiostatic transient at finite H. The steady-state and early-stage asymptotes, Eqs. (11) and (15), seem to provide quantitative predictions for the related time domains. We matched these two known asymptotes for $T \to 0$ and $T \to \infty$, by extending the formula (6) that follows from the concept of convective wave and fits well the transient data in the region of $H > 1$. The resulting semi-empirical formula contains no additional empirical parameters:

$$N(T) = \begin{cases} \beta_0 + T^{-1/2}(1 + \frac{1}{2}(T/T_0)^{3/2}); & T < T_0 \\ 1 + \beta_\infty; & T > T_0 \end{cases},$$

$$T_0^{-1/2} = \frac{2}{3}(1 + \beta_\infty - \beta_0). \tag{17}$$

The coefficients β_0 and β_∞ are known functions of H that converge to zero for $H \to \infty$, see Eqs. (11) and (16).

2.5. Corrections on geometric imperfections

Theory of the potentiostatic transient process in DL approximation operates, for ED probes of any convex shape [11], with two effective geometric parameters A, h. The only additional effective geometric parameter in a generalized semi-empirical representation (17) of the full 3D theory (finite H) is the perimeter length P, which appears in the Oldham asymptote through β_0 in (15). Small deviations from ideal shape of an ED circular probe, consisting of m members of the same nominal radius R, can be included into the effective geometric characteristics A, h, P or the related corrections κ_A, κ_P, κ_H that should be close to unity:

$$A = \kappa_A m\pi R^2, \quad P = \kappa_P m4\pi R, \quad h = \kappa_H 2bR. \tag{18abc}$$

In the present experiments, all the ED probes consist of a pair of working electrodes, $m = 2$.

For geometrically imperfect shape of an ED probe, these parameters can be determined in a purely geometric way, e.g. from their frontal photographs. Another way of deducing the effective geometric parameters $\{A, h, P\}$ consists in fitting the model (17) on a collection of primary transient data obtained with a suitable electrolyte solution for known values of wall shear rate γ. Actual A and P can be determined from the early-stage asymptote (Oldham) and actual h from the steady-state asymptote, corrected on edge effects (Leveque). Such a primary calibration includes also an indirect determining of D, based on the overall set of treated transient data.

3. Experimental

The purpose of this experimental study is to check:

- autocalibration variant [6] of the electrodiffusion flow diagnostics;
- prediction [7] of steady-state mass-transfer coefficients at finite H, Eq. (11);

- semi-empirical model of the potentiostatic transient at finite H, Eq. (17).

The present ED transient experiments cover the range $1 < H < 10^3$ of modified Peclet number. Four circular ED probes with nominal radii R embracing the range 0.1–1 mm are used together in all the transient experiments. Wall shear rate γ in the range 0.5–200 s^{-1} is adjusted by changing rotation speed Ω in a Couette viscometric cell. Diffusion coefficient D of the ferricyanide depolarizer is varied in a range 4×10^{-11}–7×10^{-10} $m^2\,s^{-1}$ by changing glycerol content in aqueous electrolyte solutions.

3.1. Solutions

Aqueous solutions of glycerol were prepared from distilled water, glycerol (dynamite grade), and electrolytes of p.a. grade: $K_4Fe(CN)_6\cdot 3H_2O$ as the cathodic (working) depolarizer, $K_3Fe(CN)_6$ as anodic (auxiliary) depolarizer, and K_2SO_4 as supporting electrolyte for enhancing conductivity and suppressing solubility of atmospheric oxygen. The steady voltamperic measurements in such electrolyte solutions display nearly ideal LDC cathodic plateau between −0.65 and −0.85 V, with changes of i_{std} below 0.5% and inflection point with $\mathrm{d}\ln i/\mathrm{d}U \approx 0.02\ V^{-1}$ at $U = -0.8$ V. Basic glycerol–water solutions were prepared volumetrically. The approx. volumetric content of glycerol in percents is used for the naming: GL00 (water), GL20 (20% of glycerol), etc. The resulting mass fraction of glycerol in basic solutions, w, is given in Table 1. Kinematic viscosity ν was determined using suitable Ubbelohde capillary viscometers at 20 and 25 °C, density ρ was determined at 22 °C using 100 ml pycnometer. The thermal viscosity factor α was calculated from the viscosity data according to its definition,

$$\alpha \equiv -\mathrm{d}\ln\nu/\mathrm{d}T. \tag{19}$$

The composition, density, and viscosity data of individual solutions are given in Table 1. The experimentally determined mechanical properties do not differ too much from the tabular data for the corresponding binary systems water–glycerol.

3.2. ED cell

Overall setup for ED measurements in steady viscometric flow with easy-controllable wall shear rate is shown in Fig. 4a. In a commercial rotational viscometer of Couette type, with inner rotating cylinder of radius $R_{in} = 18.80$ mm, the outer cylindrical vessel of radius $R_{out} = 20.00$ mm was replaced with a cylindrical ED cell of the same radius, see Fig. 4b. Nominal wall shear rate at surface of the cell is calculated from well-known Couette formula,

$$\gamma = \Omega 2\kappa^2/(1-\kappa^2), \quad \kappa \equiv R_{in}/R_{out} = 0.940. \tag{20}$$

The whole stainless body of the cell serves as the electrically grounded auxiliary electrode, compare with Fig. 1. Each of the four ED probes consists of two working electrodes of the same R, made from a platinum wire and placed on opposite sides of the cell, to suppress fluctuations due to the run-out of rotating inner cylinder. The platinum wires were first electrolytically covered with an insulating layer, then glued with epoxy resin into the borings in the wall of outer cylinder, and manually polished. Frontal photographs of the working electrodes are shown in Fig. 5. The final effective geometric characteristics of ED probes, determined from the calibration experiments, are given in Table 2.

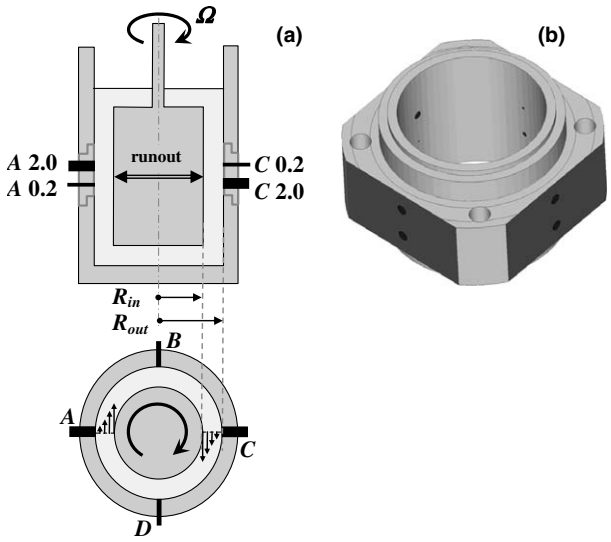

Fig. 4. ED cell: (a) overall installation using rotational viscometer with coaxial cylinders and (b) cylindrical ED cell with the ED probes, listed in Table 2.

Table 1
Composition of the solutions and properties at reference temperature 22 °C

Solution	GL00	GL20	GL30	GL40	GL50	GL60
w (kg/kg)	0	0.237	0.347	0.452	0.553	0.649
K_2SO_4 (kg l^{-1})	0.04	0.02	0.02	0.02	0.02	0.02
$K_4Fe(CN)_6\cdot 3H_2O$ (mol m^{-3})	25.00	25.00	25.00	25.00	20.00	20.00
$K_3Fe(CN)_6$ (mol m^{-3})	25.00	25.00	25.00	25.00	20.00	20.00
$10^{12}\overline{D}$ ($m^2\,s^{-1}$)	681 ± 9	348 ± 7	228 ± 5	142 ± 2	87.3 ± 0.9	45.3 ± 0.6
α (K^{-1})	0.0217	0.0260	0.0314	0.0348	0.0385	0.0450
$10^6\,\nu$ ($m^2\,s^{-1}$)	0.990	1.836	2.758	4.302	7.155	13.270
ρ (kg l^{-1})	1.008	1.087	1.092	1.121	1.128	1.189

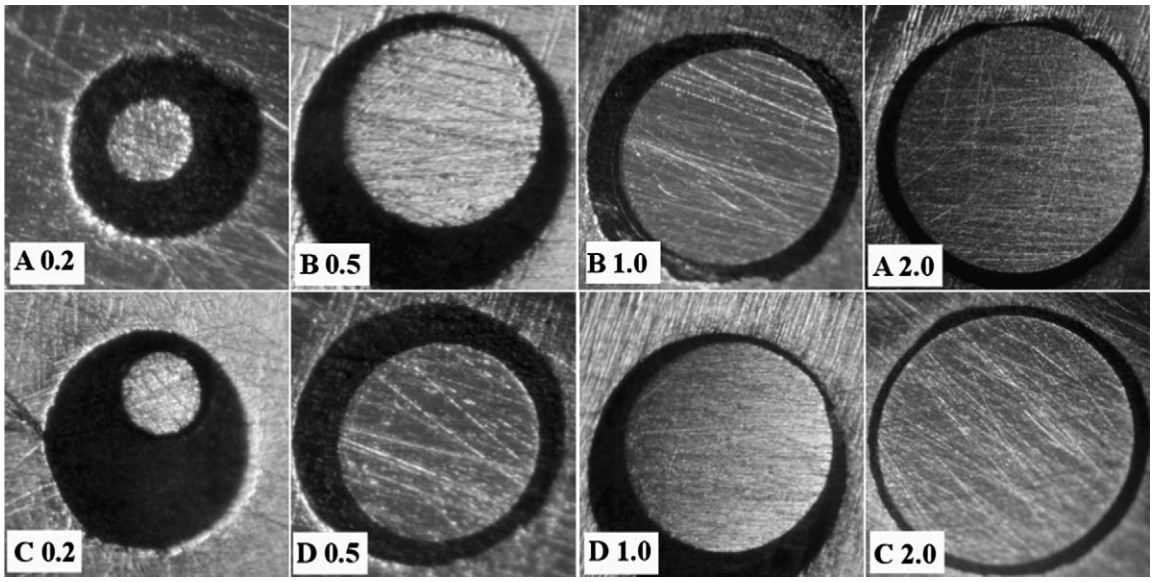

Fig. 5. Front photographs of individual working electrodes (arbitrary magnification). The notation corresponds to data on geometry in Table 2. Actual flow direction along the working electrodes is horizontal, from left to right.

Table 2
Geometry of probes according to calibrations

Probe	S02	S05	S10	S20
Working electrodes	A0.2 + C0.2	B0.5 + D0.5	B1.0 + D1.0	A2.0 + C2.0
R (mm)	0.1	0.25	0.5	1.0
κ_A	1.049	1.002	0.999	0.995
κ_P	1.100	1.050	1.020	1.010
κ_H	1.115	1.104	1.091	0.997

3.3. ED transients: process control and data acquisition

All the ED probes were driven by the common voltage U, using a multi-channel ED interface (the potentiostat and current follower) with 12-bit AD/DA converter, as described in [6]. Time schedule of a single transient experiment is shown in Fig. 6. It consists of a preparation period with adjusting the equilibrium voltage of zero-current regime, the potentiostatic transient period, and a recovery period. The zero-current regime has been achieved by adjusting a suitable equilibrium voltage U_0 between the grounded stainless auxiliary electrode and the platinum working electrodes (a few mV) in a feedback regime. The potentiostatic transient is started at $t = 0$ by the voltage step on a constant value $U_\infty \approx -0.8$ V, selected according to previous quasi-steady voltamperic measurements. Overall duration Δt of transient or recovery period can be safely estimated from the model (17) to be $\Delta T \approx 3$, i.e.

$$\Delta t \approx Dk_{\mathrm{L}}^{-2} \approx 1.5D^{-1/3}(h/\gamma)^{2/3}. \tag{21}$$

Ranges $i_{\max}$ of the bipolar current followers for individual probes are adjusted to the values that ensure accurate reading of the steady-state current but do not restrict too much the high transient currents in an early stage of the transient process. Sampling density is varied between 100 Hz and 1 kHz to cover the transient time according to (21) with maximum of 1000 points. Synchronized transient data for all four ED probes are written for a subsequent automated treatment to text files as a table of the t–i data.

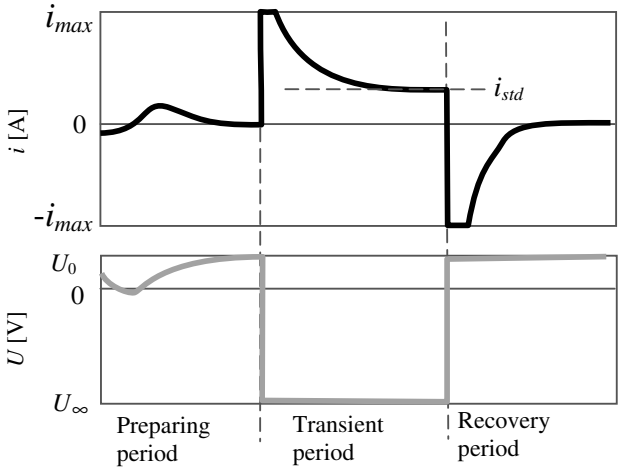

Fig. 6. Time regimes of the potentiostatic transient experiment: U (V) – controlled voltage between working and auxiliary electrode; i (A) – detected current, used also for the feedback potentiodynamic control; U_0 – equilibrium voltage guaranteeing zero current; U_∞ – cathodic overvoltage guaranteeing steady-state LDC regime; $i_{\max}$ – current range (sensitivity) of the bipolar ED interface [5]; i_{std} – steady-state current.

4. Analysis

4.1. General scheme of the data treatment

Transient records for each of four ED probes and each of six solutions were run at twenty different rotation

speeds. Their treatment was carried out in an iterative way on two levels:

- *Individual* treating a single transient, which gives an estimate of $\{D,\gamma\}$.
- *Global* treating of $\{D,\gamma\}$ estimates for all transients, which gives optimized estimates $\{\bar{\kappa}_A,\bar{\kappa}_P,\bar{\kappa}_H\}$ for each probe and average $\overline{D}$ for each solution.

In treating an *individual* transient record, the model (17) with given $\{R,\kappa_A,\kappa_P,\kappa_H\}$ and only two adjustable parameters $\{C,k_L\}$ is fitted on the selected transient t–i data. Optimizing process minimizes the root mean square of the relative deviations of i. The given $\{\kappa_A,\kappa_P,\kappa_H\}$ and $\{C,k_L\}$ for individual transients can be recalculated to $\{D,\gamma\}$ according to the autocalibration procedure, see (2) and (3). Note that, because of a specific parameter sensitivity, the combination $\kappa_A C$ depends exclusively on an early stage of transient according to (2) and, with fixed $\{\kappa_A,C\}$, the combination γ/κ_H depends exclusively on the steady-state asymptote of transient according to (3).

From the 100–1000 points, recorded for an individual transient with a constant sampling frequency, a subset is selected with approximately equidistant dividing on the $\log t$ scale. Automatically eliminated are the points with the currents exceeding 90% of the ceiling i_{max}, as well as the points from the initial stage, $t < t_{min}$. Threshold t_{min} is specific both for the probe and solution but independent of γ. Additional t–i points can be eliminated manually during the treatment. All the untreated points nevertheless remain a part of the stored transient data and can be recovered manually or by changing t_{min} in a next iteration. Excluded from the global treatment were also the entire transient records that displayed, after cutting-off the wrong data from the initial stage, the standard deviation above 2.5%. According to these criteria, approx. 5% from the overall set of 480 transients were excluded.

The *global* level of data treating aims at determining the effective geometric parameters $\{\bar{\kappa}_A,\bar{\kappa}_P,\bar{\kappa}_H\}$ of all ED probes by minimizing χ^2, the relative difference between individual estimates of $\{D,\gamma\}$ and their global counterparts $\{\overline{D},\gamma_{nom}\}$:

$$\chi^2 = \langle 4(D/\overline{D}-1)^2 + (\gamma/\gamma_{nom}-1)^2\rangle. \quad (22)$$

Here, $\langle\cdots\rangle$ stands for an average from all the treated individual records (approx. 470) and γ_{nom} are the known nominal values according to (20). $\overline{D}$ gives the average of individual estimates of D for each solution, $\{\bar{\kappa}_A,\bar{\kappa}_P,\bar{\kappa}_H\}$ for each probe give the optimum estimates of $\{\kappa_A,\kappa_P,\kappa_H\}$ that minimize χ^2. Coefficient 4 in (22) is introduced because of different sensitivity of i_L to the related parameters $\{D,\gamma\}$ in (1).

ED cell in the present design cannot be thermostated. Resulting individual values of D for an actual temperature from the interval 20–25 °C were recalculated to the reference temperature 22 °C, using the viscosity–temperature data and the correlation formula

$$vD = \text{constant}, \quad (23)$$

i.e. $\mathrm{d}\ln D/\mathrm{d}T = \alpha$, see (19).

4.2. Initial stage of transient: time threshold

Transient mass-transfer model (17) at extremely short times predicts zero transport resistances and, consequently, it must be wrong below some time threshold, $t < t_{min}$. In addition to the neglected electrochemical transport resistances, there is also a current-enhancing effect due to extremely thin diffusion layer that copies the rough surface of the working electrode. Unfortunately, available models of these concurring effects [18–20] are limited to uniformly accessible configurations and, as we tested in preliminary analyses, they cannot be applied to the present problem. Transient data from this *initial stage* should be eliminated by introducing reasonable estimates of t_{min}. The estimates of t_{min}, given in Table 3, were obtained manually, by observing systematic deviations of the initial stage of the transients for all combinations of probes and solutions. The current enhancement due to surface roughness is most obvious for the solution GL60 with lowest D (the thinnest diffusion layer) and probe S20 with largest R (the weakest Oldham edge effect), see Fig. 7.

4.3. Early stage of transient: Oldham asymptote

It follows from comparing the model (17) with its early-stage asymptote (15) that there is only a small effect of convection, below 2%, on the transient currents for $i(t)/i_{std} > 2$. This lower bound for transient currents can be taken as a delimitation of the early stage of transient, where the transient data can be treated, using the Oldham asymptote as an empirical formula,

$$t^{1/2} i(t)/(c_B n\mathbf{F}m\pi R^2) = (D/\pi)^{1/2}\kappa_A + \kappa_P D R^{-1} t^{1/2}, \quad (24)$$

linear in coordinates $t^{1/2}k(t)$ vs. $t^{1/2}$ and containing two adjustable parameters, $D^{1/2}\kappa_A$ and $D\kappa_P$. Because of extremely low sensitivity of these two parameters on the part of transient data above the early stage, the least-square fitting of the complete transient model (17) results in nearly the same estimates of $D^{1/2}\kappa_A$ and $D\kappa_P$.

4.4. Steady state: effect of free convection

Steady-state mass-transfer coefficients at very low or zero γ are affected by the concentration-driven natural convection. The present data on natural convection (zero γ) mass-transfer coefficients at low Ra to a vertical circular sink are well-correlated by

Table 3
Estimates of t_{min} for all probes and solutions

t_{min} (s)		Solution					
		GL00	GL20	GL30	GL40	GL50	GL60
Probe	S02	0.02	0.03	0.03	0.03	0.04	0.05
	S05	0.04	0.06	0.06	0.06	0.08	0.10
	S10	0.06	0.09	0.09	0.09	0.12	0.15
	S20	0.08	0.12	0.12	0.12	0.16	0.20

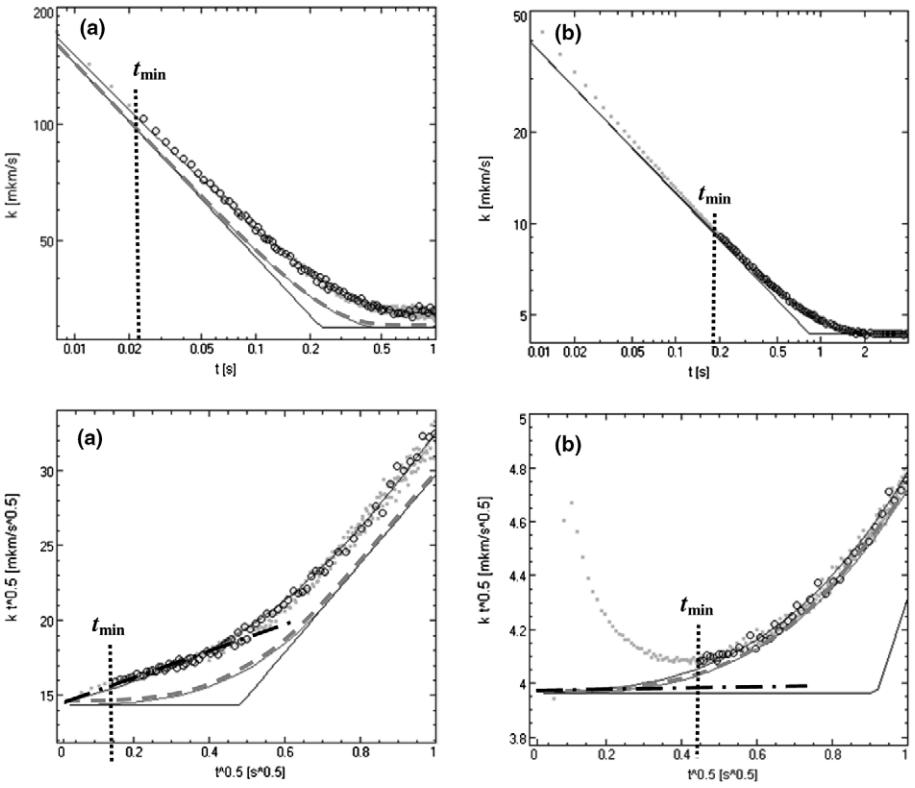

Fig. 7. Typical instances of the transients in k–t and $t^{1/2}k$–$t^{1/2}$*mappings*. Solid circles – the treated points. Small gray points – untreated part of data. Thin solid lines – best fit by the model (17). Dashed thick gray lines – the corresponding DL approximation. Dot-and-dashed thick black lines – Oldham asymptotes. Dotted vertical straight line – t_{min} thresholds. Pair of thin straight lines – Cottrell and Leveque asymptotes. (a) Small probe (S02) and solution with high D (GL00), $H = 9.8$: slight surface-roughness effect masked by a well-developed Oldham asymptote. (b) Large probe (S20) and solution with low D (GL60), $H = 803$: pronounced surface-roughness effect for $t < 0.2$ s.

$$Sh_0 \approx ((8/\pi)^4 + 0.24Ra)^{1/4}, \tag{25}$$

where the Rayleigh number $Ra = (2R)^3 g(\nu D)^{-1}(\Delta\rho/\rho)$, $g = 9.81\ \mathrm{ms}^{-2}$, and $\Delta\rho/\rho = f_B c_B$, for the present electrochemical system is taken from [21], $f_B = 5.9\mathrm{E}{-5}\ \mathrm{m}^3\ \mathrm{mol}^{-1}$. In agreement with the formula (25), the relative effect of natural convection is roughly the same for all the studied solutions as they display approximately the same values of $(\nu D)^{-1}(\Delta\rho/\rho)$.

The transients with steady-state Sh smaller than twice of the related Sh_0 were taken as affected by natural convection and excluded from the treatment.

4.5. Calibration

The adjustment of $\{\kappa_A, \kappa_P, \kappa_H\}$ by fitting the model (17) with two free parameters $\{D, \gamma\}$ on individual transient data with the aim to minimize the global χ according to (22) is nothing but a comparative geometry calibration of the ED probes.

The starting local estimates of D for each transient record were made under assumption of ideal geometry, $\{\kappa_A, \kappa_P, \kappa_H\}=\{1,1,1\}$ and displayed standard deviation about 2%. Standard errors of the corresponding global estimates $\overline{D}$ for each solution were higher, about 5%. The first estimates of $\{\bar\kappa_A, \bar\kappa_P\}$ were made manually, using in an obvious way the local estimates $D^{1/2}\kappa_A$ and $D\kappa_P$ according to the linearized Oldham asymptote (24). In an analogous way, the first estimates of $\bar\kappa_H$ were made, using the Leveque asymptote in the autocalibration version (3):

$$\bar\kappa_A = \langle (D/\overline{D})^{1/2}\rangle \kappa_A^*, \quad \bar\kappa_P = \langle D/\overline{D}\rangle \kappa_P^*,$$
$$\bar\kappa_H = t\langle \gamma_{\mathrm{nom}}/\gamma\rangle \kappa_H^* \kappa_A^*/\bar\kappa_A. \tag{26abc}$$

Here, $\langle\cdots\rangle$ stand for an averaging over all transients for a given probe and $\{\kappa_A^*, \kappa_P^*, \kappa_H^*\}$ give the estimates of geometry parameters used in the previous local treatment. The starting χ according to (22) was about 12%. Optimization of $\{\kappa_A, \kappa_P, \kappa_H\}$ consists in iterative using of (26abc). After four steps of such iteration, χ according to (22) dropped to 6%. The corresponding optimized $\{\bar\kappa_A, \bar\kappa_P, \bar\kappa_H\}$ are given in Table 2. The final local estimates of γ display almost normal distribution of relative deviations, with standard relative error about 4% for all ED probes and tested solutions. Note that such an accuracy of the γ-reading with correct $\{\bar\kappa_A, \bar\kappa_P, \bar\kappa_H\}$ would correspond to the primary experimental data on χ_C and k_{std} with accuracy about 1%. The resulting geometry characteristics $\{\bar\kappa_A, \bar\kappa_P, \bar\kappa_H\}$ are given in Table 2, the diffusion coefficients $\overline{D}$ (including the standard deviations) in Table 1.

5. Results and discussion

5.1. Correction on edge effects at finite Peclet number

The model prediction of $1+\beta_\infty(H)$ according to [7], see (11), is compared in Fig. 8 with experimental values $k_{std}/k_L = i_{std}/i_L$, calculated from actual steady-state value i_{std} of a given transient experiment and theoretical prediction of i_L according to (1) and (18ab) with $D=\overline{D}$, $\{\kappa_A, \kappa_P, \kappa_H\} = \{\bar{\kappa}_A, \bar{\kappa}_P, \bar{\kappa}_H\}$, for each solution and probe. The standard deviation of $1+\beta_\infty$ is below 2%. For a few points at lowest H, there is a systematic deviation +3%, most probably because of a slight effect of free convection.

An analogous experimental ED study of steady-state mass transfer at small Peclet number was made for 2D strip-shaped sinks [22]: a series of nine annular probes, with h ranged from 0.0016 to 5.5 mm, was built in the wall of a horizontal pipe. The experiments, made with an aqueous solution of equimolar potassium ferri/ferro-cyanide depolarizers and high concentration of KOH, were analyzed taking a rough estimate of D from an older correlation [21]. The estimated errors of Sh and Pe, calculated from primary data, were about 7%. The study [22] is limited to rather high shear rates and achieves extremely low Peclet numbers by using probes with extremely small h (below 10 μm). Because the smallest h were determined by compar-

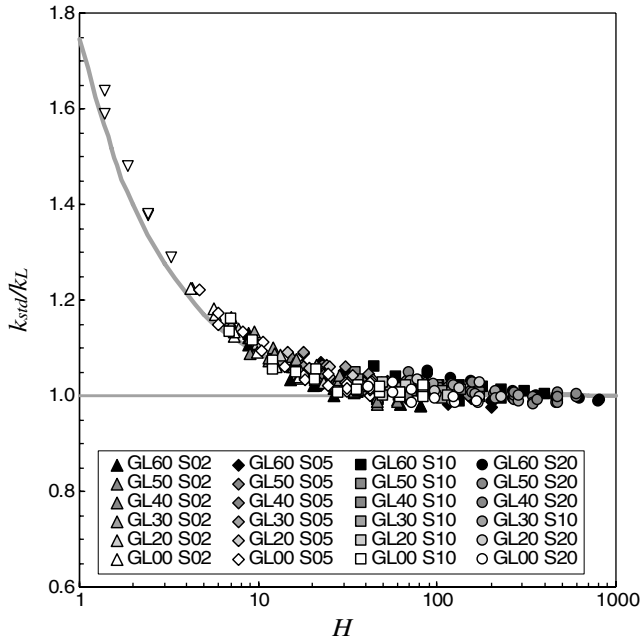

Fig. 8. Checking the prediction [7] of 3D edge effects for a circular sink in shear flow. *Curve*- empirical formula (11) from [7], fitting the numerical solution; *Points*- experimental data for four ED probes and six solutions, see Tables 1 and 2. Excepting a part of the series for GL00 and S02 (solution GL00, probe diameter 0.2 mm) with $1.5 < Sh/Sh_0 < 2$ (flipped triangles ▽), only the experimental runs with $Sh/Sh_0 > 2$ are included.

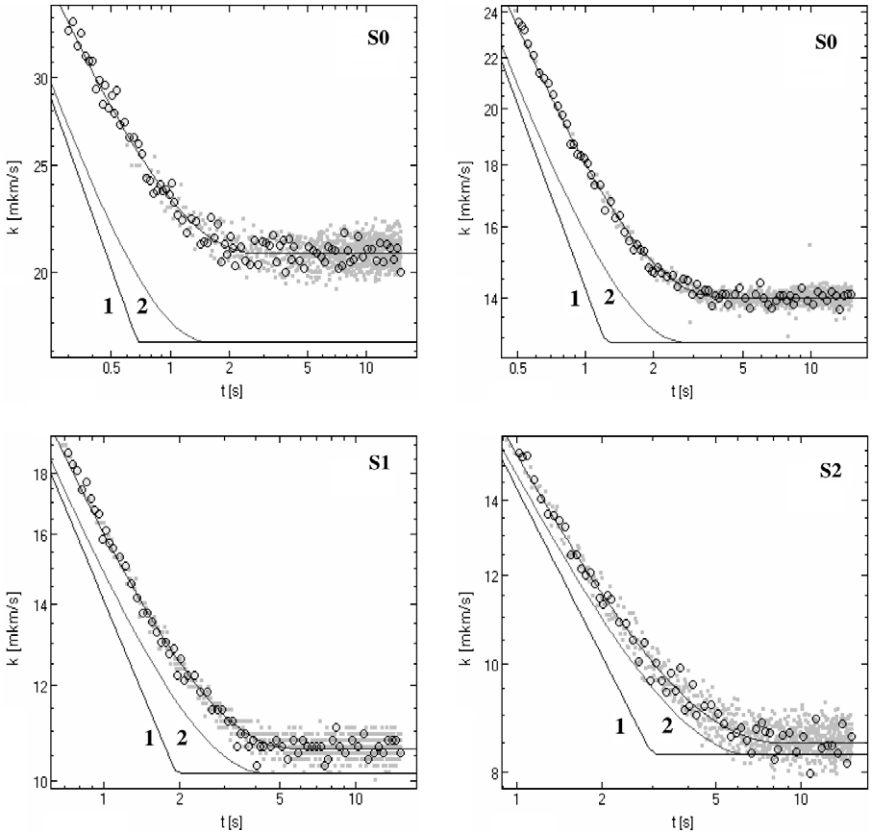

Fig. 9. Fitting the model (17) on well-behaved transient data for solution GL00 *at* $\gamma = 4\ s^{-1}$. Identification of the probes {S02, S05, S10, S20} is given in Table 2. 1 – Cottrell asymptote; 2 – DL asymptote; empty circles – treated points; small gray rectangles – untreated points. The instances cover a wide range of Peclet numbers, $H = \{4.2, 10.6, 21.1, 42.1\}$.

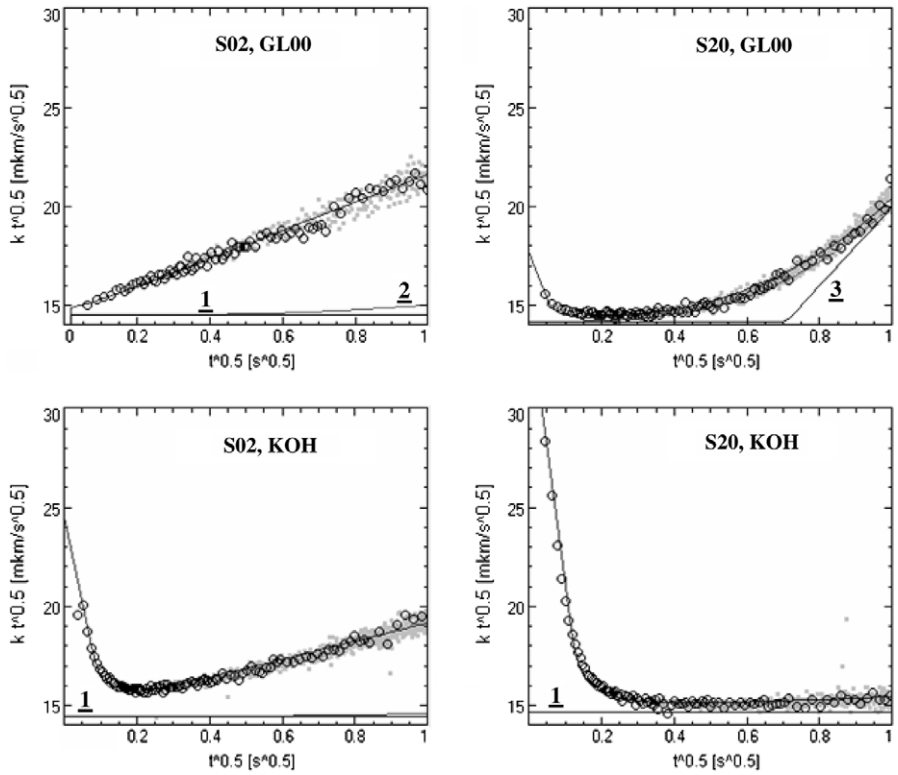

Fig. 10. Effect of supporting electrolyte on transient in the initial stage. GL00 – solution with K_2SO_4 as a supporting electrolyte, see Table 1; KOH – solution with the same depolarizer and 1 mol/l KOH as a supporting electrolyte; S02 and S20 – the probes according to Table 2; 1 – Cottrell asymptote; 2 – DL asymptote; 3 – steady state; empty circles – treated points; small gray rectangles – untreated points.

Table 4
Effect of electrolyte composition on surface-roughness parameters for selected combinations probe-solution, see Tables 1 and 2

	Probe S02		Probe S20	
	δ_S (μm)	E_0	δ_S (μm)	E_0
Solution GL00	0.7	1.02	1.4	1.25
Solution KOH	1.7	3.0	2.4	5.0

ing k_{std} of different probes at a same, sufficiently high γ, $k_{std} \sim h^{-1/3}$, the comparison of theoretical prediction $Sh = Sh(Pe)$ with experimental data is rather a fitting than checking the theory.

5.2. Transient model

The applied transient model (17) does not reflect an exact convective-diffusion theory of the transient process. It is merely a matching of known early-stage and steady-state asymptotes. However, it fits the data very well, as shown on selected instances in Fig. 9.

The standard relative error for all the shown instances is about 2%. It is obvious from Fig. 9 that this error is due to random errors so that possible systematic local deviations of the empirical model (17) from an unknown correct theory are deep below, say, 0.5%.

5.3. Initial stage of transient

Surface roughness may strongly enhance the currents at an initial stage of transient [20], when the Cottrellian diffusion layer of thickness $\delta_C(t) = (\pi Dt)^{1/2}$ copies a rough surface and, hence, the actual active surface on microscopic level and the corresponding total flux is enhanced. Firstly we tried, instead of filtering off the initial transient data, $t < t_{min}$, to include this effect quantitatively into the model (17) by using the concept of apparent enhancement of the active area [20]. Unfortunately, additional transient measurements with the same depolarizers and another supporting electrolyte (large amount of KOH instead of K_2SO_4) shown that the enhancement due to surface roughness interferes strongly with additional electrochemical transport resistances, see Fig. 10. For this reason, the idea of quantitative modeling the surface roughness effect was abandoned in favor of cancelling the initial-stage data (below the time threshold).

The tested model [20] of the area enhancement,

$$A_{enh}(t)/A \equiv \begin{cases} Z\mathrm{Arcsin}(1/Z); \\ \quad Z > E_0/(E_0^2-1)^{1/2} \\ E_0 - ((E_0^2-1)^{1/2} - \frac{\pi}{2} + \mathrm{Arcsin}(1/E_0)); \\ \quad Z < E_0/(E_0^2-1)^{1/2}, \end{cases} \tag{27}$$

where $Z = \delta_C(t)/\delta_S$, contains two micro-geometry parameters: E_0 – maximum area enhancement, δ_S – characteristic size of the microscopic irregularities. It is shown in Fig. 10 that the model is capable to fit the roughness effect quantitatively but its parameters $\{E_0, \delta_S\}$ strongly depend on composition of the electrolyte solutions, see Table 4.

A reasonable explaining of this result lies in an interference of the surface-roughness enhancement with additional electrochemical transport resistances at very high current densities [18,19], which suppresses the enhancement more strongly for low-conductivity solutions like GL00. For the small probe S02, in addition, the enhancement is completely masked by the edge effects according to Oldham, see (24). For high-conductivity solution KOH, the enhancement is obvious even for the small probe S02 and, for the large probe S20, the currents are by several times higher than according the Cottrell asymptote for smooth surfaces. As a result, the obtained surface-roughness parameters have no direct micro-geometric meaning.

6. Conclusions

- Autocalibration variant of electrodiffusion flow diagnostics was successfully used to geometrical calibration of the probes, with the coefficient diffusion D of working depolarizer determined from the flow-independent early-stage asymptote (Cottrell–Oldham), $t > t_{min}$.
- Theoretical prediction [7] of the steady-state mass-transfer coefficients by Geshev and Safarova [7] is quantitatively confirmed by the present experiments within a reasonable accuracy of 2%. Their predictions of transient characteristics are completely wrong.
- Semi-empirical model (17) of the transient process at finite Peclet number, under negligible electrochemical transport resistances and surface roughness, fits the transient data above a threshold time t_{min} very well (estimated systematic deviations below 1%).
- Available theoretical models of the electrochemical transport resistances at initial stage, $t < t_{min}$, are limited to one-dimensional models for uniformly accessible working electrode (e.g. rotation disk electrode). More realistic 3D models are not available.

Acknowledgement

This paper refers to the work done under the grant project of GAČR, Contract No. 104/04/0826.

References

[1] T.J. Hanratty, J.A. Campbell, Measurement of wall shear stress, in: R.J. Goldstein (Ed.), Fluid Mechanics Measurements, Hemisphere Publishing, Washington, 1983.
[2] V.E. Nakoryakov, A.P. Burdukov, O.N. Kashinskii, P.I. Geshev, Electrodiffusion study of local structure of turbulent flows (Russ), Inst. Thermophysics, Novosibirsk, 1986.
[3] N.A. Pokryvaylo, O. Wein, N.D. Kovalevskaya, Electrodiffusion diagnostics of flows in suspensions and polymer solutions (Russ), Nauka i Tekhnika, Minsk, 1988.
[4] J. Newman, The fundamental principles of current distribution and mass transport in electrochemical cells, in: A.J. Bard (Ed.), Electroanalytical Chemistry, A Series of Advances, vol. 2, Marcel Dekker Inc., NY, 1973, p. 187.
[5] D.D. MacDonald, Transient Techniques in Electrochemistry, Plenum Press, NY, 1977.
[6] V. Sobolik, J. Tihon, O. Wein, K. Wichterle, Calibration of electrodiffusion friction probes using a voltage-step transient, J. Appl. Electrochem. 28 (1998) 329–335.
[7] P.I. Geshev, N.S. Safarova, Angular and transient characteristics of circular electrochemical friction probes, Int. J. Heat Mass Transfer 42 (1999) 3183–3188.
[8] J.L. Hudson, S.G. Bankoff, An exact solution of unsteady heat transfer to a shear flow, Chem. Eng. Sci. 19 (1964) 591–598.
[9] M. Soliman, P.L. Chambré, On the time-dependent Leveque problem, Int. J. Heat Mass Transfer 10 (1967) 169–180.
[10] O. Wein, On the transient Leveque problem with an application in electrochemistry, Collect. Czech. Chem. Commun. 46 (1981) 3209–3220.
[11] O. Wein, V. Sobolík, Dynamics of ED friction probe I. Shape-dependent potentiostatic transient, Collect. Czech. Chem. Commun. 62 (1997) 397–419.
[12] S.C. Ling, Heat transfer from a small isothermal spanwise strip on an insulated boundary, Trans. ASME – J. Heat Transfer 85 (1963) 230–236.
[13] C.G. Phillips, Heat and mass transfer from a film into steady shear flow, Quart. J. Mech. Appl. Math. 43 (1990) 135–159.
[14] O. Wein, Lateral edge effect in electrodiffusion measurement of wall shear stress, Collect. Czech. Chem. Commun. 53 (1988) 1678–1687.
[15] H.A. Stone, Heat/mass transfer from surface films to shear flows at arbitrary Peclet number, Phys. Fluids A 1 (1989) 1112–1122.
[16] K.B. Oldham, Edge effects in semi infinite diffusion, J. Electroanal. Chem. 122 (1981) 1–17.
[17] K. Aoki, J. Osteryoung, Diffusion-controlled current at the stationary finite disk electrode, J. Electroanal. Chem. 122 (1981) 19–35.
[18] O. Wein, Effect of ohmic losses on potentiostatic transient response of reversible redox system, J. Appl. Electrochem. 21 (1991) 1091–1094.
[19] O. Wein, Voltage-step transient process at large overpotential (Russ.), Elektrokhimyia 29 (1993) 8–10.
[20] O. Wein, F.H. Assaf, Potentiostatic transient diffusion to solid electrodes with rough surfaces, Collect. Czech. Chem. Commun. 52 (1987) 848–866.
[21] J.R. Selman, J. Newman, Free convection mass transfer with supporting electrolyte, J. Electrochem. Soc. 118 (1971) 1070–1078.
[22] R.C. Ackerberg, R.D. Patel, S.K. Gupta, The heat/mass transfer to a finite strip at small Peclet numbers, J. Fluid. Mech. 86 (1978) 49–65.